Flare Physics with the Nobeyama Radioheliograph and RHESSI

A. Nindos
Section of Astrogeophysics, Physics Department, University of Ioannina, Ioannina GR-45110, Greece
anindos@cc.uoi.gr

Abstract

In this article I review the present status of knowledge in areas of special interest for further study using solar flare observations at microwaves from the Nobeyama Radioheliograph and hard X-ray (HXR) observations from RHESSI. The most direct tracers of the electrons accelerated in a flare are the microwave and HXR emissions they produce. The combined microwave and hard X-ray data provide powerful diagnostics of the physical conditions in flaring regions and particularly the magnetic field configuration of the flare and the properties of the energetic electrons. I point out that in order to tackle better the fundamental problem of particle acceleration in solar flares, detailed comparison of the spatial and spectral data with models is needed.

Key words: Sun:corona, Sun:flares, Sun:radio radiation, Sun:X-rays

1. Introduction

A solar flare is a sudden brightening in the solar atmosphere. Typically, radiation is obsreved across virtually the entire electromagnetic spectrum and all atmospheric layers are affected. It is widely believed that the energy for a flare is stored magnetically in the corona prior to the event. The key elements of a typical flare are accelerated particles, the "evaporation" of large masses of high density plasma into coronal magnetic loops and (frequently but not always) magnetic eruptions. The acceleration process yields electrons with energies much higher than the mean energy of the thermal plasma. The most direct tracers of these electrons are the hard X-ray (HXR) and microwave emission they produce.

The launch of the Reuven Ramaty High Energy Solar Spectroscopic Imager (RHESSI) on February 5, 2002 opened up a new era in high-energy solar flare physics due its unique capabilities: it observes flares over a broad range, 3 keV to 17 MeV, i. e. from thermal X-rays to gamma-rays (Lin et al. 2002). Its new approach is to combine for the first time in HXRs high-resolution imaging with high-resolution spectroscopy. Combining RHESSI data with microwave data provides a powerful tool for further progress in flare physics. Among the various radio instruments, the Nobeyama Radioheliograph (NoRH) is the only one which is solar dedicated and provides high spatial resolution images at two frequencies (17 and 34 GHz) with subsecond time resolution for flare events (Nakajima et al. 1994).

The purpose of this article is not to give an exhaustive treatment of flare microwave and HXR emissions. There is already a number of reviews that cover all aspects of microwave flare emission (Kundu & Vlahos 1982; Alissandrakis 1986; Bastian, Benz, & Gary 1998) and HXR emission (Sakao 1994; Hudson & Ryan 1995; Aschwanden 2002). Also a review about the complementarity of microwave and HXR emission has been published by Gary (2000). Here, I will only try to give a comprehensive account of our present knowledge in areas of special interest for further study using combined NoRH and RHESSI data. To this end, I will try to convince the reader that detailed modeling is required in order to exploit the wealth of information provided by the NoRH and RHESSI data.

2. Morphology of HXR and Microwave Emissions

2.1. HXR Sources

Both HXR and microwave flare emissions come from energetic electrons. However, the emission mechanisms at these wavelength ranges are radically different. The HXRs come from bremsstrahlung and there are two general classes of models for the HXR emission from solar flares (e.g. see Hudson, Canfield, & Kane 1978; Tandberg-Hanssen & Emslie 1988; Raulin et al. 1999). In the "thin target" model, the nonthermal electrons are very effectively trapped in the corona and produce HXRs via bremsstrahlung on the ambient coronal ions: in that case the HXR photon spectral index γ is related to the electron energy spectral index δ_x by $\delta_{x,thin} = \gamma - 0.5$. In the "thick target" model, the nonthermal electrons are trapped in closed magnetic loops, where the ambient density is sufficiently low that collisions are ineffective in changing the electron energies. In this case the bulk of the HXRs are produced via bremsstrahlung when the nonthermal electrons strike the dense chromospheric material at the footpoints of the coronal loop, and

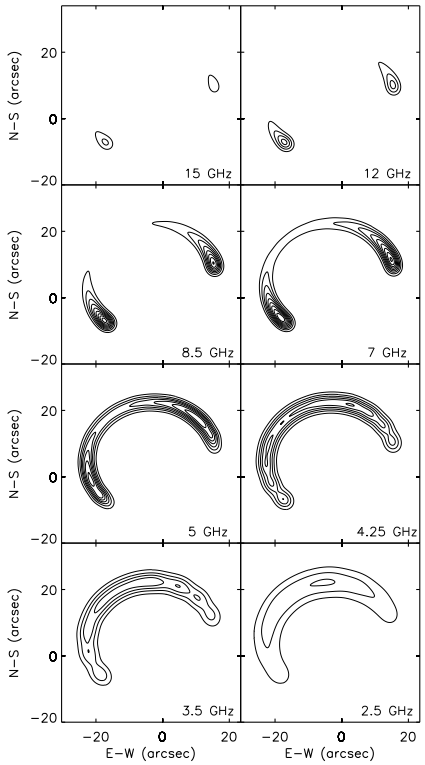

Fig. 1. Gyrosynchrotron model loop calculations at several frequencies. The model is a magnetic loop located at heliographic longitude 50° and latitude 50° north and with a 45° orientation with respect to the local north. The footpoint magnetic field strength is 700 G. The heights above the solar surface of the two lines of force that form the loop are 22″ and 9.5″. The distance between the footpoints is 36″ and the loop transverse dimension is 10″. The energy spectral index of the energetic electrons is 3 and their density is 6×10^6 cm^{-3}. The low- and high-energy cutoffs of the nonthermal electrons are 10 and 500 keV, respectively.

$\delta_{x,thick} = \gamma + 1.5$.

Using Yohkoh's Hard X-ray Telescope (HXT) Sakao (1994) has established that the dominant HXR morphology is the double source, although single compact sources or multiple components are also seen. Of the double sources for which magnetograms are available, the two sources lie on opposite sides of the magnetic neutral line. The study of simultaneous soft X-ray, H_α,and HXR images (e.g. Kosugi et al. 1992; Sakao et al. 1992) shows that the double HXR sources are located at the footpoints of flaring loops (to clarify the description, by the term "loop" I mean a collection of adjacent magnetic field lines sharing a common morphology and adjacent footpoints. Thus, a "single loop" does not mean a single field line; since magnetic field lines have no thickness, there must be infinitely many field lines in a loop of finite volume, and the field lines within the loop may have unresolved structure). Note also that the magnetically weaker footpoint is brighter in HXRs than is the magnetically stronger footpoint (Sakao 1994; Kundu et al. 1995). The above observational picture indicates that impulsive phase HXR emission is dominated by thick-target bremsstrahlung emission by nonthermal electrons. A further argument supporting the thick-target interpetation is that quantitative agreement between microwave and HXR emission during the rise phase of impulsive flares, including the numbers of electrons required (Gary 1985; Lu & Petrosian 1989; Chiuderi-Drago et al. 1998), is only possible if nonthermal thick-target radiation dominates the HXR emission.

2.2. Microwave Sources

On the other hand, the microwaves originate from the gyrosynchrotron mechanism as the energetic electrons spiral along magnetic fields in the corona. The morphology of the microwave flare emission depends on the magnetic field configuration (i.e. the geometry of the flaring region and its location on the disk) and the properties of the nonthermal electrons. In order to show how the magnetic field affects the microwave emission, in fig. 1 I present models of gyrosynchrotron loop emission for typical magnetic field and energetic electron parameters at several frequencies (similar models have been developed by Preka-Papadema & Alissandrakis 1992; Bastian, Benz, & Gary 1998). At high frequencies the emission is compact and optically thin and comes from the footpoints of the loop, and most strongly from the high-field end of the loop. At lower frequencies, the radio emission becomes optically thick and there is a tendency for more extended sources, indicating emission from the entire loop. This picture is consistent with the properties of gyrosynchrotron mechanism: the magnetic field is much stronger near the footpoints, which favors

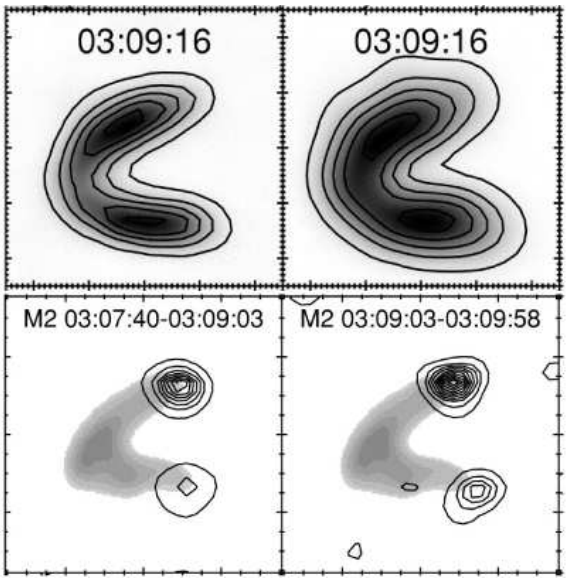

Fig. 2. Images of a flare in radio and X-rays during the impulsive phase. The top row shows radio images at 34 (left panel) and 17 (right panel) GHz total intensity with contours at 10%, 30%,...,90% of the maximum overlaid on gray-scale images of the 17 GHz total intensity. The bottom row shows Yohkoh HXT M2 channel HXR images overlaid on the gray-scale representation of the SXT image of the period 03:11:00-03:11-54 UT (from White et al. 2002).

the higher frequencies. A decrease of the frequency of observation has approximately the same effect as an increase of the magnetic field. Thus when the frequency of observation decreases, we expect to have emission not only from the footpoints but also from a significant part of the loop. Note that in fig. 1, the centroid of the radio emission moves progressively down toward the footpoints at higher frequencies. This effect has been oberved in Owens Valley Solar Array (OVSA) data studied by Wang et al. (1995; 1996). In addition to the role of magnetic field strength in radio emission, there is a strong dependence on magnetic field direction, with the emission coming most strongly from regions where the magnetic field is perpendicular to the line of sight.

As for the nonthermal electrons, Bastian, Benz, & Gary (1998) have pointed out that a magnetic loop acts as a dispersive element: at a fixed frequency higher energy electrons emit at the loop top (weak magnetic field) and lower energy electrons emit at the footpoints (strong magnetic field). This is due to the dependence of mean energy E of the gyrosynchrotron-emitting electrons on the magnetic field strength B and the spectral index of the electron distribution function δ ($E \propto B^{-(0.5+0.085\delta)}$). Furthermore, changing the parameters of the nonthermal electrons the microwave emission is affected as follows. Changing the number density has little effect in the optically thick limit but in the optically thin limit has the same effect as increasing the magnetic field. As for the electron energy cutoffs, imposing an upper limit to the electron energies present in the distribution has a strong suppression effect on radiation at high frequencies which requires very energetic electrons if the magnetic field is not strong. Increasing the low-energy cutoff has little effect on the high-frequency emission since the low-energy electrons do not radiate significantly at high frequencies, but it increases the mean energy of the electrons radiating the optically thick emission and makes it brighter.

Here a word of caution is needed: in the model of fig. 1, I have assumed that the microwave-emitting electrons have uniform density and isotropic pitch angle distribution. This is a zero-order approximation but it is justified by the fact that e.g. in a loss-cone distribution, the electrons missing are those with small pitch angles whose gyroacceleration and hence emissivity is smallest. Most of the emission is produced by the larger pitch angles, so using an isotropic distribution should not affect the results significantly. Furthermore such models with isotropic density and pitch angle distributions are able to reproduce the properties of the microwave emission of some flares *at the peak of the event*: one compares the radio observations with gyrosynchrotron model loop calculations. The best-fit model should satisfy two criteria: (1) the projection of the model loop shape on the plane of the sky should be consistent with the appearance of the flaring loop; and (2) the resulting model radio emission should reproduce both the observed fluxes and structures at the peak of the event. We have been able to derive a self-consistent model for the magnetic field and the properties of the nonthermal electrons for two events. The first was observed at 5 and 15 GHz with the VLA and additional spectral data were provided by the OVSA (Nindos et al. 2000) and the second was observed with the NoRH at 17 and 34 GHz with spectral data from the Nobeyama Polarimeter (Kundu, Nindos, & Grechnev 2004). However, there are certainly flares whose microwave emission can be interpreted only if one considers an anisotropic population of nonthermal electrons. One particular class of such flares is the events which are optically thin but their maximum

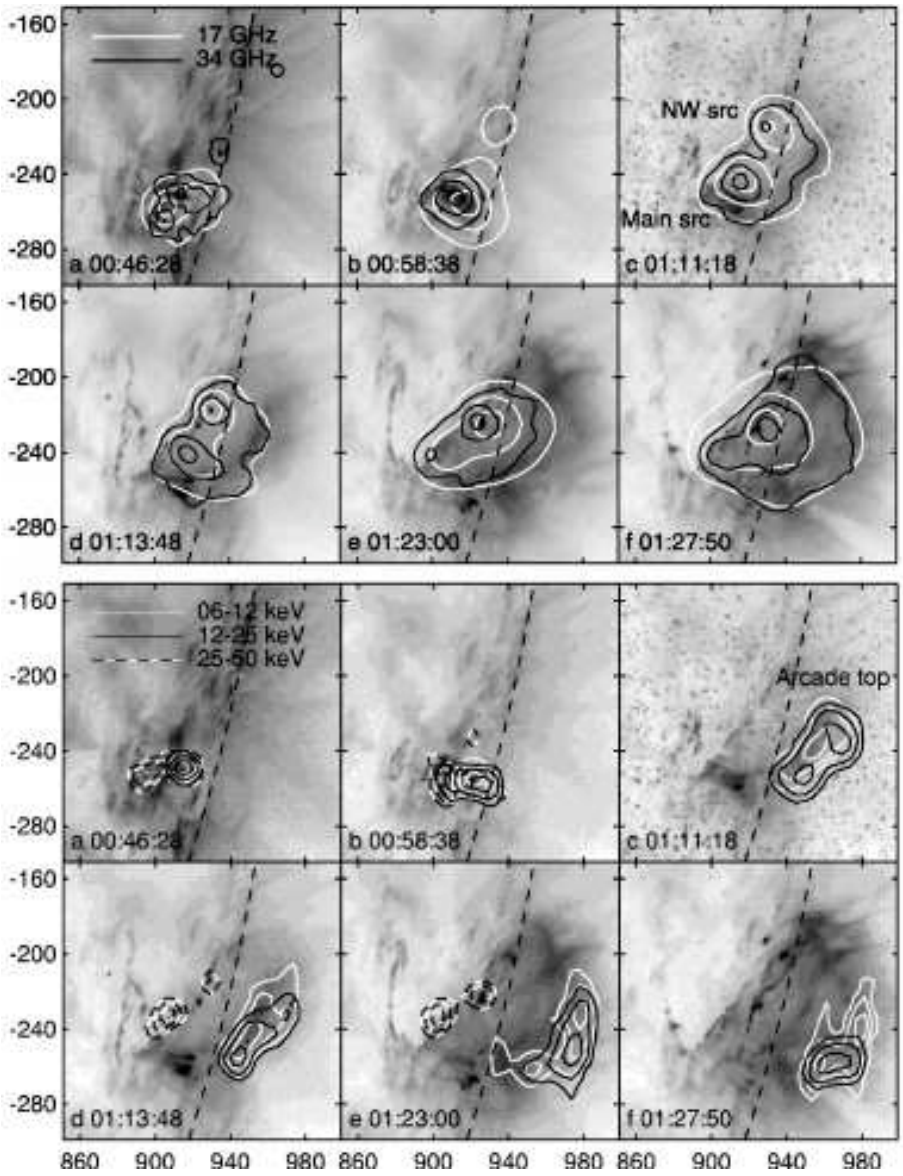

Fig. 3. A flare observed by NoRH and RHESSI. In the two top rows, a sequence of overlays of 17 (white contours) and 34 (black contours) GHz images on TRACE 195 Å Fe XII images (inverted color table) during the flare's main phase. Contour levels are at 10%, 40%, and 80% of the maximum in each image. The two bottom rows show sequence of overlays of RHESSI HXR images overlaid on the TRACE images appearing in the two top rows. 6-12 keV images are shown in white contours, 12-25 keV images in black contours, and 25-50 keV images in dashed contours. Contour levels are at 10%, 40%, and 80% of the maximum in each image (from Kundu et al. 2004).

microwave emission comes from the loop-top (see section 4.1).

2.3. Overall View

From a practical point of view, the analysis presented in sections 2.1 and 2.2 indicates that HXR images and single-frequency radio images may look quite different, and the appearance of the radio images will change depending on frequency. An example, obtained from the study by White et al. (2002), is given in fig. 2: the microwave emission at 17 and 34 GHz covers the whole loop as it is demarcated by the soft X-ray image while the HXR sources are located at the footpoints of the loop.

Simultaneous morphological studies of flares in HXRs, soft X-rays, and microwaves, together with photospheric magnetograms have provided valuable information about the flare configuration over the years. The first such high-resolution observations were published by Alissandrakis, Schadee, & Kundu (1988). Here I do not attempt to cite all relevant literature; the interested reader may refer to the review by Bastian, Benz, & Gary (1998). I only mention the articles by Nishio et al. (1997) and Hanaoka (1996; 1997; 1999) who analyzed NoRH data. Nishio et al. (1997)

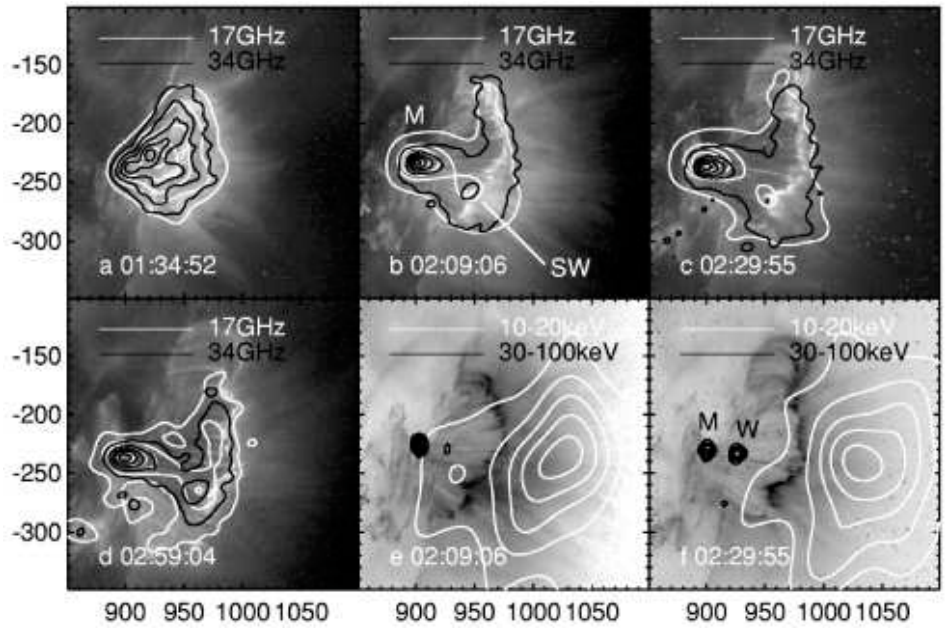

Fig. 4. Evolution of the radio and HXR sources later in the flare presented in fig. 3. The first four images show a sequence of overlays of 17 (white contours) and 34 (black contours) GHz images on TRACE 195 Å Fe XII images during the extended phase of the flare when the loop system is expanding above the west limb. The upper four contour levels are at 30%, 50%, 70%, and 90% of the maximum in each image, while the lowest contours are at 10%, 4%, 2%, and 1%, respectively. The last two images show contours of the RHESSI 10-20 keV (white) and 30-100 keV (black) emission overlaid on TRACE 195 Å Fe XII images (from Kundu et al. 2004).

found that most of the flares they studied involved at least two coronal loops: one loop is compact while the other is larger. Both loops have 17 GHz emission while HXRs are emitted preferentially by the more compact of the two loops. Similarly, soft X-ray emission is brighter in the compact loop. Hanaoka also studied the double-loop configuration flares and found that the compact loop is associated with the emergence of a parasitic magnetic polarity within the active region. These studies indicate that interacting loops of different sizes may give rise to a significant number of flares. Furthermore, configurations involving more complex loop systems also exist (e.g. see the early VLA observations analyzed by Kundu et al. 1982).

2.4. NoRH-RHESSI Observations of a Complex Event

As an example of a complex flare configuration, in figures 3 and 4, I present NoRH and RHESSI observations of an X1 flare analyzed by Kundu et al. (2004). Of course a detailed description of the event cannot be given here due to its complexity; the interested reader is referred to the article by Kundu et al. (2004). The main flare starts after 01:08 UT and the microwave emission consists of several components (see fig. 3). The strong components appearing in panels (c)-(d) have clear HXR counterparts from 01:13 UT onward. The energy distribution in the impulsive phase inferred for the radio-emitting electrons is quite similar to that inferred for the HXR-emitting electrons. After the main phase of the flare, the morphology of the radio sources has changed significantly (see fig. 4). Kundu et al. (2004) identified around 01:38 UT at least four regions showing different temporal behavior. Note that even after the main phase of the flare, the sources M and SW of fig. 4 are nonthermal. The combined radio and HXR data for this event reveal a remarkable diversity of energy release and nonthermal acceleration sites.

3. Electron Dynamics

3.1. Trapping and Precipitation

Most of the morphological studies of the HXR and microwave emission have focused on images obtained at the peak of the event. As we discussed in §2, such studies may provide important diagnostics of the magnetic field and the properties of the nonthermal electrons. But concerning the acceleration process, they merely imply that the HXRs come from the "precipitating component" of the accelerated population while microwaves come from the "trapped component": at the simplest level the acceleration of electrons is regarded as a process that injects the electrons onto magnetic field lines at a time dependent rate. There is always a critical pitch angle, the loss-cone angle α_0, such that electrons with smaller pitch angles are not reflected by the magnetic field as they approach the footpoints. Some

fraction of the electrons are injected with pitch angles lying in the loss-cone and precipitate on their first appoach to the footpoint. The remaining fraction is injected with pitch angles outside the loss-cone and remain trapped in the corona unless pitch angle scattering takes place.

In order to refine the above picture, detailed timing studies are required. In a series of papers, Aschwanden and colleagues (Aschwanden, Schwartz, & Alt 1995; Aschwanden et al. 1996a; 1996b; 1996c) have performed timing studies of HXR data in the energy range of 25-200 keV and demonstrated that the energy-dependent time delays of fast time structures (on time scales less than a few seconds) are consistent with time-of-flight differences, while the smoothly varying HXR flux shows delays of opposite sign that are consistent with electron collisional deflection times. This behavior of the HXR timing has been interpreted (e.g. Aschwanden 1998) in the framework of the "trap-plus-precipitation/direct precipitation" model (TPP/DP): electrons with initially small pitch angle ($\alpha \leq \alpha_0$) precipitate directly to the HXR emission site while electrons with initially large pitch angles ($\alpha \geq \alpha_0$) are temporarily trapped and precipitate after the collisional deflection time.

The identification of direct precipitation in microwaves has begun only recently (Kundu et al. 2001a; Lee et al. 2002). Kundu et al. (2001a) compared the radio time profiles of two simple spiky bursts observed with NoRH at 17 and 34 GHz with a trap model derived using the Yohkoh HXT 53-93 keV time profile. Each microwave time profile was modeled as the sum of a component identical to the hard X-ray time profile (the injection function) and a trapped component derived by intergrating over the injection function convolved with an exponential kernel function. The equation for the radio flux due to the trapped population alone is an integral over the trapped particle energy distribution convolved with the synchrotron emissivity. Furthermore the microwave emission from the directly precipitating electrons will not have the same emissivity as the trapped electrons since, by definition, the precipitating electrons have a different pitch angle distribution.

The above statements certainly constrain future modeling efforts of the time profile of microwave emission. Ideally, one wants to model both the observed radio flux and structures as a function of time (note that the models presented by Nindos et al. 2000 and Kundu, Nindos, & Grechnev 2004 deal with radio observations at the peak of the event only). In general, one *cannot* use the HXR time profile as an injection function for the radio-emitting electrons, let alone the radio flux profile itself which requires an integration over energy convolved with the synchrotron emissivity.

The current status of modeling the time profile of microwave emission exploits the information provided by radio spectra. When the emission is optically thin, the microwave spectrum is a direct measure of the electron energy distribution and can be used as a tool for exploring electron evolution in phase space (Petrosian 1981; Dulk & Marsh 1982). In general an observed radiation spectrum represents a combination of acceleration and the transport effect, which cannot, in general, be separated. However, in the case where the transport process is dominated by Coulomb collisions, we may possibly separate one from the other, as the involved physics is well known. Lee & Gary (2000) selected an event for which they were sure that was dominated by Coulomb collisions. They identified their event as dominated by Coulomb collisions from the observed spectral flattening and microwave morphology in comparison with magnetic field. Lee & Gary (2000) were able to explain the temporal evolution of the microwave spectrum of their event if Coulomb collisions act on an initial narrow pitch angle distribution. Of course, it is fair to say that many events show evidence of more extreme pitch angle diffusion than can be provided by Coulomb collisions.

3.2. Microwaves and HXRs Come from the Same Population Of Electrons?

The discussion in §3.1 suggests that microwave emission and HXR emission have different properties and therefore do not necessarily come from the same population of electrons. However, it is often said that both emissions come from the same population of electrons. It has long been assumed that, because the time profiles of HXR and microwave emission are so similar (Kundu 1961) and because of the tight correlation between peak fluxes in the two emissions (e.g. Kosugi, Dennis, & Kai 1988), the "same" electrons are responsible for the two emissions. Of course, the ultimate proof whether radio-emitting and hard X-ray-emitting electrons are energized by the same acceleration process, requires a demonstration that they have the same energy spectrum and a consistent timing in both wavelength ranges. Here, I give some qualifications on this issue.

First of all, even spatially unresolved observations sometimes show that the time of maximum flux at microwaves lags behind the time of HXR maximum flux by 1-3 sec (Crannell et al. 1978). Also microwave emission usually decays more slowly than the HXR emission. Usually the observed microwave delays are interpreted in the framework of efficient trapping: under Coulomb collisions, high-energy electrons live longer than low-energy electrons. Therefore the energetic electrons producing microwaves remain in the flaring loop longer and the microwaves they produce peak later than the HXRs which come from lower energy electrons. Bastian, Benz, & Gary (1998) refined these results by analyzing flares observed simultaneously by NoRH at 17 GHz and the BATSE instrument on board the Compton Gamma Ray Observatory (CGRO). Using spatially unresolved data, the relative HXR/microwave timing agreed with earlier studies. When the timing comparisons were made using the spatially resolved 17 GHz images, they found that the microwave delay varied significantly within the source with footpoint microwave emission showing the minimum delay with respect to HXRs and loop-top emission showing the largest delays. Such variation of delays within a flaring loop are due to energy-dependent effects (at a given frequency the microwave loop-top emission comes from electrons

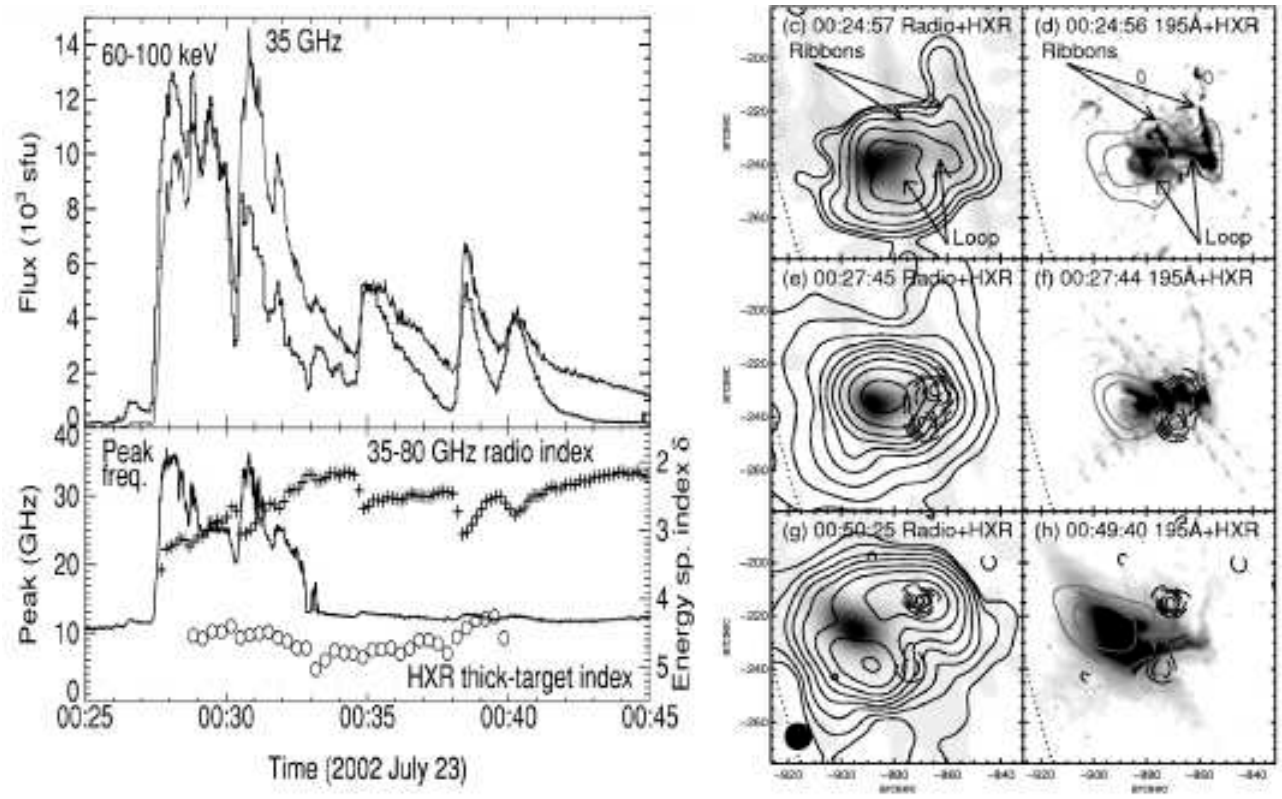

Fig. 5. Left panel, top: comparison of the RHESSI 60-100 keV HXR light curve and the NoRP 35 GHz light curve. Left panel bottom: time evolution of the radio spectral peak frequency (solid curve) and the radio spectral index from 35 to 80 GHz converted to an electron energy spectral index (plus signs). For comparison, the thick target electron energy spectral index from the RHESSI 100-400 keV spectrum is also shown (circles). Right panel: Images of the flare at X-ray, EUV, and radio-λ. The left frames show the RHESSI gray-scale image of 12-20 keV overlaid with 17 GHz contours (solid curves) and 100-150 keV HXR contours. The right frames show a 195 Å image of the same region overlaid with solid gray contours for the 12-20 keV HXRs and dashed black contours for the 100-150 HXR (from White et al. 2003).

with higher energies than those giving footpoint emission).

Furthermore, discrepancies between the electron spectral indexes inferred from microwave and HXR data during the impulsive burst phase have been reported occasionally (e.g. Kundu et al. 1994; Raulin et al. 1999). Silva, Wang, & Gary (2000) studied the statistical properties of 27 flares and found that in 75% of the bursts, the inferred index of the electron energy distribution of the microwave-emitting electrons, δ_r, is harder than that of the lower energy HXR-emitting electrons, δ_x, on average by 0.5-2.0. This implies that there is a breakup in the energy spectra of the electrons. The difference between δ_r and δ_x may be explained either by two different electron populations being accelerated in different sites with distinct physical conditions or in the framework of the "trap-plus-precipitation" model. This model predicts a hardening of the spectra of the trapped electrons because of the losses of lower energy electrons by energy-dependent Coulomb collisions (Trottet & Vilmer 1984). In this case, the microwaves produced by the electrons in the trap reflect this hardening while the HXR spectra produced by the precipitated electrons preserve the original injection spectrum, which is softer.

3.2.1. Microwave and HXR Imaging of High-energy Electrons

RHESSI offers us the opportunity, for the first time, to image HXRs produced by electrons at photon energies above 100 keV. Therefore using simultaneous NoRH and RHESSI observations we can compare the emissions from electrons in the same energy range at two different wavelength regimes. The first such comparison was published by White et al. (2003) (see fig. 5). Note that the gyrosynchrotron mechanism is very efficient and allows us to detect electrons with energies of hundreds of keV even in small flares. On the other hand, flares in which HXRs above 100 keV can be imaged do not happen so often, because the steeply falling power-law spectra do not yield sufficient photons at high energies for image formation.

Fig. 5 (right panel) shows the structure of the radio and HXR sources (the maximum 17 GHz brightness temperature exceeds 10^9 K!). The left panel of fig. 5 indicates that the radio and HXR time profiles are so similar, that one cannot argue that radio emission comes from a long-lived population of trapped electrons while the HXRs come from directly

precipitating electrons as it occurs in other events. The radio and HXR-emitting electrons should have a common origin. Fig. 5 also shows that the peak frequency of the radio spectrum reaches values as high as over 35 GHz. The energy spectral index derived from the 35-80 GHz spectra is $\delta_r \approx 1.6 - 1.8$ which does not agree with the value derived from the 40-400 keV HXRs, which is $\delta_x \approx 4.5$. White et al. (2003) were forced to conclude that a single population of electrons with a power law index of 4.5-5 above 100 keV produces the emission at 17 and 34 GHz if one assumes that the 35-80 GHz spectral index does not reflect the true optically thin value. Both radio and HXR data require extreme densities of electrons to be accelerated in the energy release: over 10^{10} cm^{-3} above 20 keV! Clearly, a systematic search in the RHESSI database is required in order to check whether or not similar events with sufficient photons at such high energies exist. If they do exist, comparing the resulting HXR images with NoRH data will be interesting.

4. Anisotropies/Deviations From the Classical Picture

The discussion in §2, assumed that the microwave-emitting electrons have uniform density and isotropic pitch angle distribution. However, there is ample evidence, both at microwaves and HXRs/gamma-rays, that in some flares the energetic electrons are distributed anisotropically. First of all, there is the prominent directivity of gamma-ray flares (McTiernan & Petrosian 1991) produced by relativistic electrons. Furthermore, Lee & Gary (2000) found that anisotropic pitch-angle distribution (including anisotropic injection) is required for explaining the spectral evolution of a flare at microwaves (see §3). Fleishman & Melnikov (2003a, 2003b) have studied both the optically thin and optically thick gyrosynchrotron emission produced by energetic electrons with anisotropic pitch angle distributions. They found that the properties of the emitted radiation (intensity, optically thin spectral index, degree of polarization) depend sensitively on the type and degree of electron anisotropy. Lately, significant attention has been paid to optically thin loop-top microwave sources as evidence for electron anisotropies.

4.1. Optically Thin Microwave Loop-top Sources

Kundu et al. (2001b) analyzed three limb flares observed with the NoRH at 17 and 34 GHz. The flare geometry was simple with one well-defined flaring loop in each event. The 17 and 34 GHz emissions were optically thin and peaked close to the loop tops. As has been shown by many studies (e.g. Alissandrakis & Preka-Papadema 1984, Preka-Papadema & Alissandrakis 1992, Bastian, Benz, & Gary 1998, Nindos et al. 2000) an optically thin loop in which the magnetic field declines from the footpoint to the loop top will generally be brightest at the footpoints of the loop if the density and pitch angle distribution of the nonthermal electrons are uniform. The angle between the magnetic field and the line of sight also plays an important role, but for the events studied by Kundu et al. (2001b) this angle is expected to be large everywhere along the loop since the flares took place close to the limb. Kundu et al. (2001b) were forced to invoke a magnetic field with constant strength along the loop in order to partly reconcile the observations with gyrosynchrotron loop models like the one presented in §2. This is consistent with studies of nonflaring loops in the EUV and soft X-rays that show little change in the apparent thickness of loops from footpoint to loop top (Klimchuk 2000; Watko & Klimchuk 2000).

A magnetic configuration with little magnetic field variation along the loop creates obvious problems in the trapping of the radio-emitting electrons. Melnikov, Shibasaki, & Reznikova (2002) suggest that the loop top sources in optically thin events are due to the highly inhomogeneous distribution of the energetic electrons along the flaring loop: accelerated electrons are concentrated in the upper part of the loop. This interpetation is supported from timing studies employed by Melnikov et al. (2002): (1) The loop-top emission is delayed by several seconds with respect to the footpoint emission and this delay is more pronounced at 34 than at 17 GHz; (2) the time profile of the loop top emission is wider and its decay slower than those of the footpoint emission; (3) on the other hand, there is almost no delay between the emissions from the regions close to the footpoints. Melnikov, Shibasaki, & Reznikova (2002) considered the question whether the anisotropic distribution of electrons along the loop is due to the acceleration/injection process or due to transport effects. Their simulations seem to support the idea that the high concentration of electrons at the loop top is due to transeverse pitch angle anisotropy of the injected electrons. But they also point out that transport effects (enhanced pitch angle scattering and energy losses near the footpoints due to either higher plasma density in the lower part of the loop or enhanced level of whistler turbulence) can yield a similar morphology. If the transport effects dominate one may expect that at the beginning of the flare the regions closer to the footpoints will be brighter than the loop top. Of course the combination of both acceleration/injection and transport mechanisms is also possible.

Overall, the NoRH data imply that the existence of flares with highly anisotropic distribution of energetic electrons is undeniable. However, we do not know how often such events occur. A statistical study of the properties of the optically thin limb flares observed by the NoRH may shed some light on this question. Note however, that the results of such study may show ambiguites due to the fact that NoRH is not able to resolve the total intensity structures of some flares (e.g. see Kundu et al. 2001a).

4.2. HXR Coronal Sources

The existence of impulsive HXR coronal sources located above the soft X-ray flaring loop is one of the most spectacular discoveries of the Yohkoh mission. This phenomenon is refered to as the "Masuda flare" (Masuda 1994; Masuda et al. 1995) and has attracted significant attention. The Masuda source occurs during the impulsive phase of a flare but appears to be unusual, in that surveys (Aschwanden 2002) only revealed a handful of such events among Yohkoh's many flares. Since the Masuda events have been observed in limb flares we are confident that the coronal HXR brightening is not due to projection effects. The production of HXRs by bremsstrahlung is proportional to the product of the densities of the ambient thermal electrons and the nonthermal electrons. In order to have a coronal source other than by projection effects, one of these densities must peak at the location of the coronal source. In the case of the Masuda flares, there is no plasma density enhancement at the location of the HXR coronal source; therefore it seems to require trapping of the nonthermal electrons there, possibly due to a combination of large pitch angles for the nonthermal electrons and a strong gradient in magnetic field strength from the top of the loop to the bottom in order for magnetic mirroring to be effective (Fletcher & Martens 1998; Metcalf & Alexander 1999).

Masuda et al. (1995) interpreted their discovery as evidence of magnetic reconnection above the soft X-ray flaring loop. The interpretation was done in terms of the so-called "standard reconnection model" (Carmichael-Sturrock-Hirayama-Kopp-Pneuman model, CSHKP) involving a fast-mode MHD shock terminating the reconnection outflow. The HXR coronal source could arise in particle acceleration either at the shock itself via the Fermi mechanism, with trapping by the paired slow-mode shock structures present in the standard reconnection model (Tsuneta & Naito 1998). Alternatively, a stochastic acceleration model (e.g. Jakimiec et al. 1998) could also explain the presence of energy conversion above the loop top.

The Masuda above-the-loop-top sources is not the only kind of coronal HXR sources detected by the Yohkoh HXT. Tomczak (2001) studied 14 behind-the-limb flares with occulted footpoints. This is the best selection criterion if one wants to detect coronal HXR sources without the presence of strong footpoint sources which can disturb the observational features of the coronal source during the process of image reconstruction. In addition to the Masuda sources, Tomczak (2001) found HXR coronal sources cospatial with bright loop-top kernels seen in soft X-ray images. Furthermore, Hudson et al. (2001) found a moving source from an over-the-limb flare. The HXR source emerged from behind the limb as a compact structure identifiable with a microwave source and moved outwards at about 10^3 km/sec.

4.3. RHESSI Observations of HXR Coronal Sources

RHESSI with its superior sensitivity and dynamic range is a suitable instrument for the study of coronal HXR sources. Indeed several coronal sources have been detected since its launch (Jiang et al. 2004). They may appear at different phases of the flare event. According to Jiang et al. (2004), in most cases, their spectrum can be fitted with either a thermal or a power-law model. In the impulsive phase, the spectra seem to fit the power-law model better while in the decay phase the loop top sources are thermal. Balciunaite, Krucker, & Lin (2004) have observed 6 behind-the-limb flares with occulted or partially occulted footpoints and have been able to detect Masuda type above-the-loop-top HXR sources.

Veronig & Brown (2004) studied two flares with HXR emission coming mainly from the loop top and only weak footpoint emission. Both are gradual events with very steep spectra and high coronal column densities This class of HXR sources should not be confused with Masuda sources and are interpreted as "coronal thick-target flares" by Veronig & Brown (2004): the corona is collisionally thick and the energy is released due to collisions in the corona before the electrons reach the footpoints. The implied coronal density of the thermal plasma is about 2×10^{11} cm^{-3}. Both events have been observed within the Nobeyama time zone and it would be interesting to check the radio data against the RHESSI data.

One of the objectives of the RHESSI mission is to check flare reconnection models. Therefore it is not surprising that attention has been paid to the motions of coronal HXR sources: in four events, Sui & Holman (2003) and Sui, Holman, & Dennis (2004) studied the dynamics of the coronal HXR source with respect to the flaring loop and found evidence for the formation and development of a current sheet between the loop top and the coronal source.

Using suitable NoRH and RHESSI data, it will be interesting to study the relation of the mechanism producing coronal HXRs with respect to the process which yields microwave flaring loop emission.

5. Conclusions and Future Work

Two central goals of flare observations are to determine the magnetic field configuration of the flare and the characteristics of the electron population, how it evolves with time and how it relates to the injected population. Achieving progress in these areas is necessary in order to tackle better the fundamental problems of energy release and particle acceleration in solar flares.

Systematic morphological studies using data from the NoRH and RHESSI can give us important information about

the possible configurations that may give rise to energy release and particle acceleration. Using spectral data we need to determine whether the electron energy spectra derived from HXRs are consistent with those derived from microwaves; and if not what causes the discrepancy. Furthermore, in order to obtain quantitative information about the magnetic field and the nonthermal electrons in the flaring region, detailed comparison of the spatial and spectral structure of the observations with models is needed integrating all observational information available. The current gyrosynchrotron loop models are static and do not account for anisotropies of the electron population. Meaningful progress can be made only if we diagnose the anisotropies better: currently we do not know whether the anisotropies are due to acceleration and injection or due to transport effects.

Overall, we need to develop more sophisticated models to account for even the grossest of characteristics of some flares. The NoRH has been, and always will be, a valuable source of data that should be used in such projects. With the future development of the Frequency Agile Solar Radiotelescope imaging spectroscopy in radio will be achieved, resulting to even greater progress in high-energy flare physics.

Acknowledgements

I would like to thank the organizers of the "Nobeyama Symposium 2004" for their invitation and financial support. Prof. C.E. Alissandrakis and Dr. S.M. White are thanked for several fruitful discussions.

References

Alissandrakis C.E. 1986, Sol. Phys. 104, 207
Alissandrakis C.E., Preka-Papadema P. 1984, A&A, 139, 507
Alissandrakis C.E., Schadee, A., Kundu M.R. 1988, A&A, 195, 290
Aschwanden M.J. 1998, ApJ, 502, 455
Aschwanden M.J. 2002, Space Sci. Rev., 101, 1
Aschwanden M.J, Schwartz R.A., Alt D.M. 1995, ApJ, 464, 974
Aschwanden M.J, Hudson H.S., Kosugi T., Schwartz R.A. 1996a, ApJ, 464, 985
Aschwanden M.J, Kosugi T., Hudson H.S., Wills M.J., Schwartz R.A. 1996b, ApJ, 470, 1198
Aschwanden M.J, Wills M.J., Hudson H.S., Kosugi T., Schwartz R.A. 1996c, ApJ, 468, 398
Balciunaite P., Krucker S., Lin R.P. 2004, AGU-SH13A, 1131
Bastian T.S., Benz A.O., Gary D.E. 1998, ARA&A, 36, 131
Chiuderi-Drago F., Alissandrakis C.E., Bentley R.D., Philips A.T. 1998, Sol. Phys., 182, 459
Crannell C.J., Frost K.J., Saba J.L., Matzler C., Okhi K. 1978, ApJ, 223, 620
Dulk G.A., Marsh K.A. 1982, ApJ, 259, 350
Fleishman G.D., Melnikov V.F. 2003a, ApJ, 584, 1071
Fleishman G.D., Melnikov V.F. 2003b, ApJ, 587, 823
Fletcher L., Martens P.C.H. 1998, ApJ, 505, 418
Gary D.E. 1985, ApJ, 297, 799
Gary D.E. 2000, in "High Energy Solar Physics -Anticipating HESSI", ed R. Ramaty, N. Mandzhavidze (ASP Conf. Ser. 206), p. 297
Hanaoka, Y. 1996, Sol. Phys., 165, 275
Hanaoka, Y. 1997, Sol. Phys., 173, 319
Hanaoka, Y. 1999, PASJ, 51, 483
Hudson H.S., Ryan J. 1995, ARA&A, 33, 239
Hudson H.S., Canfield R.C., Kane S.R. 1978, Sol. Phys., 60, 137
Hudson H.S., Kosugi T., Nitta N.V., Shimojo M. 2001, ApJ, 561, L211
Jakimiec J., Tomczak M., Falewicz R., Phillips K.J.H., Fludra A. 1998, A&A, 334, 1112
Jiang Y.W., Liu S.M., Liu W., Petrosian V. 2004, BAAS, 204, 9805
Klimchuk J.A. 2000, Sol. Phys., 193, 53
Kosugi T., Dennis B.R., Kai K. 1988, ApJ, 324, 1118
Kosugi T., et al. 1992, PASJ, 44, 45
Kundu M.R. 1961, J. Geophys. Res., 60, 4308
Kundu M.R., Vlahos L. 1982, Space Sci. Rev., 32, 405
Kundu M.R., Schmahl E.J., Velusamy T., Vlahos L. 1982, A&A, 108, 188
Kundu M.R., White S.M., Gopalswamy N., Lim J. 1994, ApJ (Suppl.), 90, 599
Kundu M.R., Nitta N., White S.M., Shibasaki K., Enome S., Sakao T., Kosugi T., Sakurai T. 1995, ApJ, 454, 522
Kundu, M.R., White S.M., Shibasaki K., Sakurai T., Grechnev V.V. 2001a, ApJ, 547, 1090
Kundu, M.R., Nindos, A., White S.M., Grechnev V.V. 2001b, ApJ, 557, 880
Kundu, M.R., Nindos, A., Grechnev V.V. 2004, A&A, 420, 351
Kundu M.R., Garaimov V.I., White S.M., Krucker S. 2004, ApJ, 1052
Lee J., Gary D.E. 2000, ApJ, 543, 457
Lee J., Gary D.E., Qiu J., Gallagher P.T. 2002, ApJ, 572, 609
Lin R.P., et al. 2002, Sol. Phys. 210, 3
Lu E., Petrosian V. 1989, ApJ, 338, 1122
Masuda S. 1994, PhD thesis, Univ. of Tokyo
Masuda S., Kosugi T., Hara H., Sakao T., Shibata K., Tsuneta S. 1995, PASJ, 47, 677
Melnikov V.F., Shibasaki K., Reznikova V.E. 2002, ApJ, 580, L185
Melnikov V.F., Reznikova V.E., Yokoyama T., Shibasaki K. 2002, in "Solar variability: from core to outer frontiers. The 10th European Solar Physics Meeting, 9 - 14 September 2002", ed A. Wilson (ESA SP-506, Noordwijk), p. 339
McTiernan J.M., Petrosian V. 1991, ApJ, 379, 381
Metcalf T.R., Alexander A. 1999, ApJ, 522, 1108
Nakajima H., et al. 1994, Proc. IEEE, 82, 705
Nindos A., White S.M., Kundu M.R., Gary D.E. 2000, ApJ, 533, 1053
Nishio M., Yaji K., Kosugi T., Nakajima H., Sakurai T. 1997, ApJ, 489, 976
Petrosian V. 1981, ApJ, 251, 727
Preka-Papadema P., Alissandrakis C.E. 1992, A&A, 257, 307
Raulin J.-P., White S.M., Kundu M.R., Silva A.V.R., Shibasaki K. 1999, ApJ, 522, 547
Sakao T. 1994, PhD thesis, Univ. of Tokyo
Sakao T., et al. 1992, PASJ, 44, L83
Silva A.V.R., Wang H., Gary D.E. 2000, ApJ, 545, 1116
Sui L., Holman G.D. 2003, ApJ, 596, L251
Sui L., Holman G.D., Dennis B.R. 2004, ApJ, 612, 546

Tandberg-Hanssen E., Emslie A.G. 1988, The Physics of Solar Flares, (Cambridge Univ. Press, Cambridge)
Tomczak M. 2001, A&A, 366, 294
Trottet G., Vilmer N. 1984, Adv. Space Res., 4(2-3), 153
Tsuneta S., Naito T. 1998, ApJ, 495, L67
Veronig A.M., Brown J.C. 2004, ApJ, 603, L117
Wang H., Gary D.E., Zirin H., Schwartz R.A., Sakao T., Kosugi T., Shibata K. 1995, ApJ, 453, 505
Wang H., Gary D.E., Zirin H., Nitta N., Schwartz R.A., Kosugi T. 1996, ApJ, 456, 403
Watko J.A., Klimchuk J.A. 2000, Sol. Phys., 193, 77
White S.M., Kundu M.R., Garaimov V.I., Yokoyama T., Sato J. 2002, ApJ, 576, 505
White S.M., Krucker S., Shibasaki K., Yokoyama T., Shimojo M., Kundu M.R. 2003, ApJ, 595, L111